





Revisiting catalytic His and Glu residues in coproporphyrin ferrochelatase – unexpected activities of active site variants

Thomas Gabler¹, Andrea Dali², Marzia Bellei³, Federico Sebastiani², Maurizio Becucci², Gianantonio Battistuzzi⁴ , Paul Georg Furtmüller¹ , Giulietta Smulevich^{2,5}  and Stefan Hofbauer¹ 

¹ Department of Chemistry, Institute of Biochemistry, University of Natural Resources and Life Sciences, Vienna, Austria

² Department of Chemistry "Ugo Schiff" (DICUS), University of Florence, Sesto Fiorentino, Italy

³ Department of Life Sciences, University of Modena and Reggio Emilia, Italy

⁴ Department of Chemical and Geological Sciences, University of Modena and Reggio Emilia, Modena, Italy

⁵ INSTM Research Unit of Firenze, Sesto Fiorentino, Italy

Keywords

enzyme activity; ferrochelatase; LC–MS; prokaryotic heme biosynthesis; resonance Raman spectroscopy; site-directed mutagenesis

Correspondence

S. Hofbauer, Department of Chemistry, Institute of Biochemistry, University of Natural Resources and Life Sciences, Muthgasse 18, Vienna A-1190, Austria
 Tel: +43 1 47654 77258

E-mail: stefan.hofbauer@boku.ac.at

G. Smulevich, Department of Chemistry "Ugo Schiff" (DICUS), University of Florence, Via della Lastruccia 3-13, Sesto Fiorentino (FI) I-50019, Italy
 Tel: +39 0554573083

E-mail: giulietta.smulevich@unifi.it

(Received 13 December 2023, revised 17 January 2024, accepted 13 February 2024)

doi:10.1111/febs.17101

The identification of the coproporphyrin-dependent heme biosynthetic pathway, which is used almost exclusively by monoderm bacteria in 2015 by Dailey *et al.* triggered studies aimed at investigating the enzymes involved in this pathway that were originally assigned to the protoporphyrin-dependent heme biosynthetic pathway. Here, we revisit the active site of coproporphyrin ferrochelatase by a biophysical and biochemical investigation using the physiological substrate coproporphyrin III, which in contrast to the previously used substrate protoporphyrin IX has four propionate substituents and no vinyl groups. In particular, we have compared the reactivity of wild-type coproporphyrin ferrochelatase from the firmicute *Listeria monocytogenes* with those of variants, namely, His182Ala (H182A) and Glu263Gln (E263Q), involving two key active site residues. Interestingly, both variants are active only toward the physiological substrate coproporphyrin III but inactive toward protoporphyrin IX. In addition, E263 exchange impairs the final oxidation step from ferrous coproheme to ferric coproheme. The characteristics of the active site in the context of the residues involved and the substrate binding properties are discussed here using structural and functional means, providing a further contribution to the deciphering of this enigmatic reaction mechanism.

Introduction

The identification of the coproporphyrin-dependent (CPD) heme biosynthesis pathway by Dailey *et al.*, [1] which is utilized almost exclusively by monoderm bacteria, is one of the major scientific discoveries of the

last decade. It leads the way to understanding the biosynthetic path of heme metabolism in many dangerous pathogens, fundamental for investigations to yield mechanism-based antimicrobial drugs [2,3].

Abbreviations

Bs, *Bacillus subtilis*; coproheme, iron coproporphyrin III; CPD, coproporphyrin dependent; CpfC, coproporphyrin ferrochelatase; cpl, coproporphyrin I; cpIII, coproporphyrin III; LC–MS, liquid chromatography–mass spectrometry; *Lm*, *Listeria monocytogenes*; MppIX, methylprotoporphyrin IX; *N*-MeMP, *N*-methylmesoporphyrin; ppIX, protoporphyrin IX; PPD, protoporphyrin-dependent; PpfC, protoporphyrin ferrochelatase; pplX, protoporphyrin IX; RR, resonance Raman; WT, wild type.

Ferrochelatases are enzymes which insert ferrous iron into a porphyrin macrocycle within heme biosynthesis pathways [4]. However, while ferrochelatases of monoderm and diderm representatives do not significantly differ from each other in their overall subunit structure and fold, they exhibit differences in the porphyrin binding site architecture [5–7]. In addition, in some ferrochelatase representatives of both monoderm and diderm bacteria (e.g., in some actinobacterial ferrochelatases or representatives of Bacteroidetes [8]), a [2Fe-2S] cluster of yet unknown function is found. The occurrence of a [2Fe-2S] cluster is not strictly correlated to phylogenetics and cannot be used to differentiate monoderm and diderm ferrochelatase sequences [8,9]. Subtle differences in conserved amino acid composition of the porphyrin binding site make diderm ferrochelatases better suited to bind protoporphyrin IX (ppIX), thus protoporphyrin ferrochelatase (PpfC), whereas monoderm representatives preferentially bind coproporphyrin III (cpIII), thus coproporphyrin ferrochelatase (CpfC). CpIII lacks the two vinyl groups of the ppIX at positions 2 and 4 and carries two propionates at these positions instead [2]. These enzymes are possibly active also with different porphyrin substrates, although with an altered efficiency, according to the different possible interaction schemes. An overview of different porphyrin structures is provided in Fig. 1A. It is worth noting that PpfCs catalyze the final step of heme synthesis in the protoporphyrin-dependent (PPD) pathway and CpfCs the penultimate reaction, but both enzymes insert ferrous iron into a porphyrin ring [2,10,11].

Prior to the identification of the CPD pathway, all prokaryotic ferrochelatases were investigated using two-propionate substrates like ppIX or mesoporphyrin IX (MppIX). These studies were mainly performed on the ferrochelatase from the monoderm firmicute *Bacillus subtilis* (*Bs*) and led to many important findings about protein structure and function [12–15]. In detail, the role of the conserved active site residues (distal glutamate and histidine) and the proximal residue, which depends on phylogeny (methionine in metazoans, tyrosine in Firmicutes, phenylalanine in actinobacteria) [2,5,16], was analyzed and mechanistically discussed with data obtained from human and yeast ferrochelatases [17–21]. The fact that phenylalanine is found on this proximal position in actinobacterial CpfCs is interesting as it cannot be a ligand for iron *per se*. The glutamate–histidine pair was identified as the iron-binding site in *Bs*CpfC and was shown to be essential for the catalysis of iron incorporation into two-propionate substrates [12]. Similarly, for the human enzyme, the same pair was shown to be the essential

acid–base couple for the initial proton abstraction of the pyrrole nitrogen atoms, necessary for the insertion of divalent metals [17,22–24]. The proximal residue was reported to determine substrate (divalent metal) specificity [14,24].

In this study, we are revisiting the active site of the coproporphyrin ferrochelatase from the firmicute *Listeria monocytogenes* (*LmCpfC*), which is defined by the conserved glutamate–histidine (H182–E263) pair (Fig. 1B). We thoroughly studied the wild-type (WT) *LmCpfC* and its H182A and E263Q variants by several biochemical and biophysical methods (UV–vis and resonance Raman spectroscopies, mass spectrometry, UV–vis spectroelectrochemistry, enzyme activity measurements), in order to determine their catalytic role in ferrous iron insertion into the physiological substrate (cpIII) and its oxidation to yield ferric iron coproporphyrin III (coproheme). An oxidation step is a precondition as in the last step of the CPD pathway coproheme decarboxylase requires a ferric coproheme to react with hydrogen peroxide to finally yield heme *b* in monoderm bacteria [25–28]. However, the mechanism of the insertion of ferrous iron by ferrochelatases to accumulate a ferric product, also under anaerobic conditions, has not been discussed extensively in the literature.

Results

Ferrous iron insertion into cpIII and ppIX

Identification of the CPD heme biosynthesis pathway opened up a new scientific chapter, questioning some conclusions from the past. Based on this novel finding, we follow the iron insertion capability into cpIII and ppIX by the WT and the two active site variants (H182A and E263Q) of the coproporphyrin ferrochelatase from the monoderm firmicute representative *L. monocytogenes* (Fig. 2) using UV–vis electronic absorption spectroscopy. When the physiological substrate (cpIII) is used, full conversion to coproheme by WT *LmCpfC* is observed using UV–vis spectroscopy. This is manifested by changes from the cpIII-bound *LmCpfC* spectrum (bands at 405, 507, 544, 560, and 611 nm) [7] to the coproheme-bound *LmCpfC* spectrum (bands at 397, 497, 527, and 618 nm) [6] (Fig. 2A). Under identical conditions, full coproheme conversion was not achieved with the H182A (Fig. 2B) and E263Q (Fig. 2C) variants of *LmCpfC*. In fact, the spectra of the variants differ in the intensities of the bands in the visible region as compared to the WT, since their resulting spectra upon titration show bands characteristic of both the cpIII-bound and

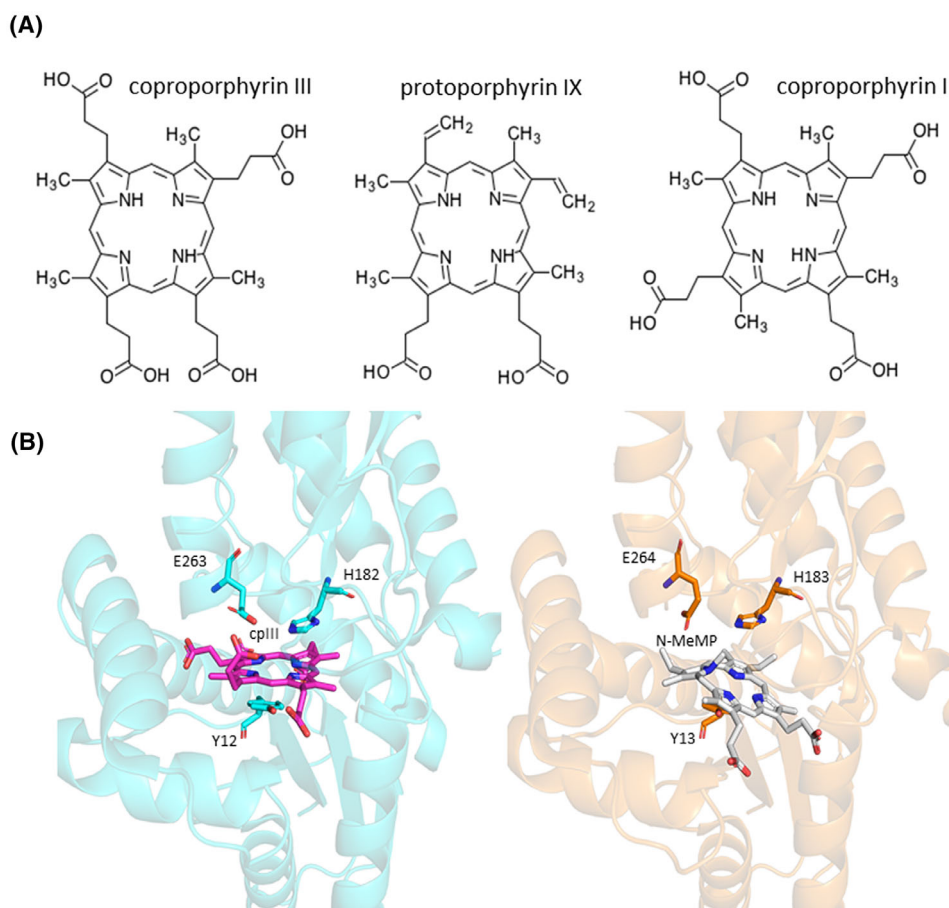


Fig. 1. Structures of porphyrins and overall *LmCpfC* structure. (A) Chemical structures of coproporphyrin III, protoporphyrin IX, and coproporphyrin I derived from the KEGG Compound database (<https://www.genome.jp/kegg/compound/>). (B) Structure of *LmCpfC* in complex with cpIII (pdb-code: 8AT8) [7]. Secondary structural elements are shown as cyan cartoon, active site residues are shown as cyan sticks, and cpIII as pink sticks. Structure of *BsCpfC* in complex with *N*-methylmesoporphyrin (*N*-MeMP) (pdb-code: 1C1H) [35], secondary structural elements are shown as orange cartoon, active site residues as orange sticks and the *N*-MeMP as gray sticks. PYMOL (<https://pymol.org/2/>) was used for structure illustration.

coproheme-bound enzymes in their ferrous and ferric forms (Fig. 3). Interestingly, the E263Q variant shows the highest content of unreacted cpIII, as well as a contribution by ferrous coproheme (Fig. 3).

Spectral transitions of WT *LmCpfC* and its variants using ppIX as a substrate give valuable insights. The WT enzyme can incorporate ferrous iron into ppIX forming heme *b*, as manifested by the change from the ppIX-bound WT *LmCpfC* spectrum (bands at 412, 510, 548, 573, and 626 nm) to the heme *b*-bound spectrum (bands at 401, 504, 532, and 621) [6], although full conversion to heme *b* is not reached. In the final spectrum of the ferrous iron titrated sample, shoulders at wavelengths characteristic of the ppIX-bound *LmCpfC* are still clearly identifiable (specifically at 510, 573, and 626 nm) (Fig. 2D). In contrast to WT

LmCpfC, both variants are unable to insert ferrous iron into the porphyrin (Fig. 2E,F). Upon the addition of ferrous iron, the spectra remain typical of those of the free-base porphyrin spectrum, except for minor variations in the Soret region. Interestingly, the symmetrical substrate coproporphyrin I (cpI), with propionate groups at positions 2, 4, 6, and 8 (Fig. 1) is also accepted for iron insertion activity by the wild-type enzyme, similar to the natural substrate (cpIII) (Fig. 4).

The resonance Raman (RR) spectra of cpIII-bound and ppIX-bound to WT *LmCpfC* together with the corresponding spectra of the free porphyrins are compared in Fig. 5. Their core size marker bands are similar to those characteristic of a six-coordinated high-spin (6cHS) metalloporphyrin species. The

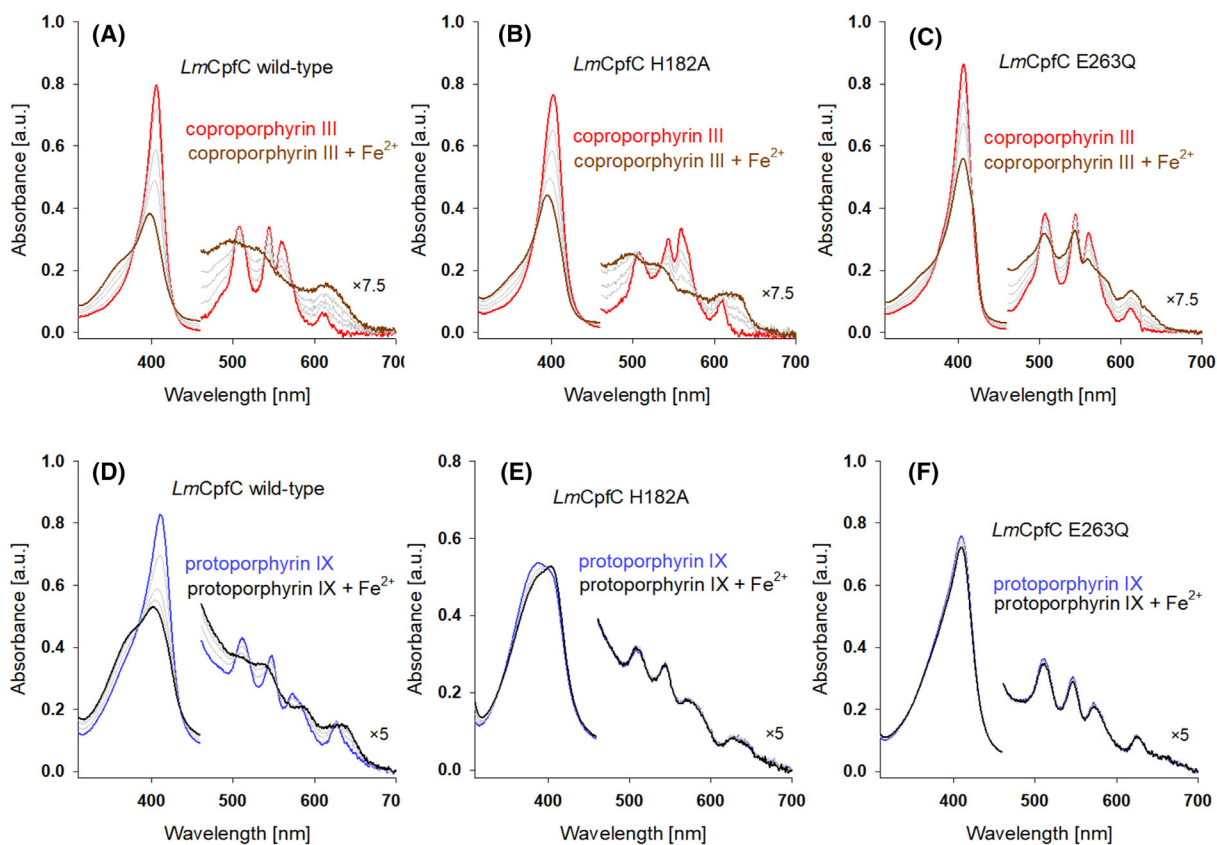


Fig. 2. Catalytic insertion of ferrous iron into cpIII and ppIX by wild type (WT) and variants of *LmCpfC* followed by UV–vis spectroscopy. Spectra of cpIII bound to (A) WT, (B) H182A, and (C) E263Q variants of *LmCpfC* are depicted in red and the final spectra after stepwise addition of 1.5-fold excess (final) of ferrous iron in maroon. Spectra of ppIX bound to (D) WT, (E) H182A, and (F) E263Q variants of *LmCpfC* are depicted in blue and the final spectra after the addition of 1.5-fold excess of ferrous iron in black. Intermediate spectra during the titration are shown in gray. Titrations have been measured in triplicates ($n = 3$), with one representative titration presented for each sample.

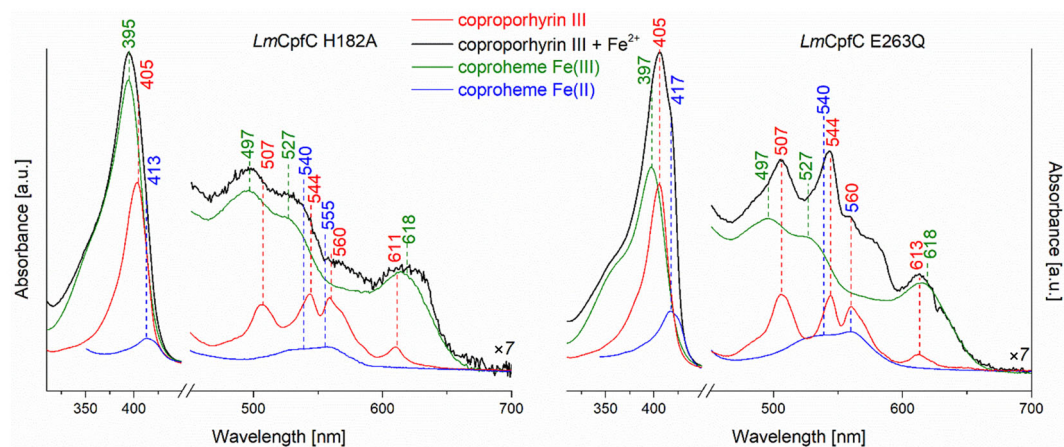


Fig. 3. Qualitative description of the final UV–vis spectra of the catalytic insertion of ferrous iron into cpIII by H182A and E263Q variants of *LmCpfC*. The spectra and the typical wavelength of the cpIII, coproheme-bound species in the ferrous and ferric forms of H182A and E263Q variants of *LmCpfC* are reported in red, blue, and green, respectively, while the final spectra of the ferrous iron titrations in black.

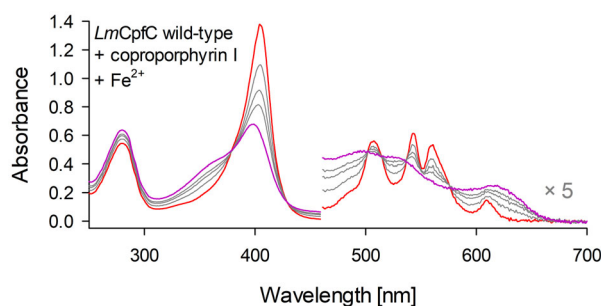


Fig. 4. Monitoring of ferrous iron insertion into coproporphyrin I catalyzed by wild-type (WT) *LmCpfC* by titration. Spectrum of cpI-bound WT *LmCpfC* is shown in red, and intermediate spectra during ferrous iron titration are shown in gray. The final spectrum (iron coproporphyrin I bound to WT *LmCpfC*) is presented in violet.

binding and substrate specificity of coproporphyrin ferrochelatase strictly depend on hydrogen-bond interactions between the propionate groups and the protein matrix. In the *LmCpfC*-cpIII complex, the RR low wavenumber region is altered, as compared to the free porphyrin, since all propionates establish hydrogen bonds to residues in the active site with different strengths, resulting in the appearance of four distinct propionate bending modes in the spectrum of the complex [7].

Binding of ppIX to WT *LmCpfC* is also confirmed by the RR signal in the low wavenumber region. The comparison of the spectra of free and *LmCpfC*-bound

ppIX indicates a readjustment of the propionate groups which shift from 360–393 to 365–373 cm^{-1} in the complex. However, upon insertion of ppIX into *LmCpfC*, the propionate interactions to the protein are weaker than in the cpIII complex, since the δ ($\text{C}_\beta\text{C}_\alpha\text{C}_\beta$) bending mode wavenumbers of the propionate groups at positions 6 and 7 are downshifted being observed at 365–373 cm^{-1} in the ppIX-*LmCpfC* complex and at 381–393 cm^{-1} in the cpIII-*LmCpfC* complex. In addition, the bending modes of the vinyl groups in ppIX appear to be slightly affected by the complexation, upshifting from 406 (free ppIX) to 409 cm^{-1} (bound ppIX).

To complement the spectroscopic observations, all samples were analyzed prior to titration and after completion of the reaction using liquid chromatography–mass spectrometry (LC–MS). This allows quantitative detection of porphyrin species that can be related to the final spectra of iron titration experiments. In Fig. 6, all chromatograms of porphyrin samples corresponding to coproheme (708.18 Da), cpIII (653.28 Da), heme *b* (616.18 Da), and ppIX (563.26 Da) are shown. While WT *LmCpfC* can completely convert cpIII into coproheme, the same enzyme can insert ferrous iron into ppIX to only approximately 35%. Quantification of coproheme, cpIII, heme *b*, and ppIX, calculated by integration of the area under the respective elution peak is presented separately in Fig. 6D for all analyzed samples. The

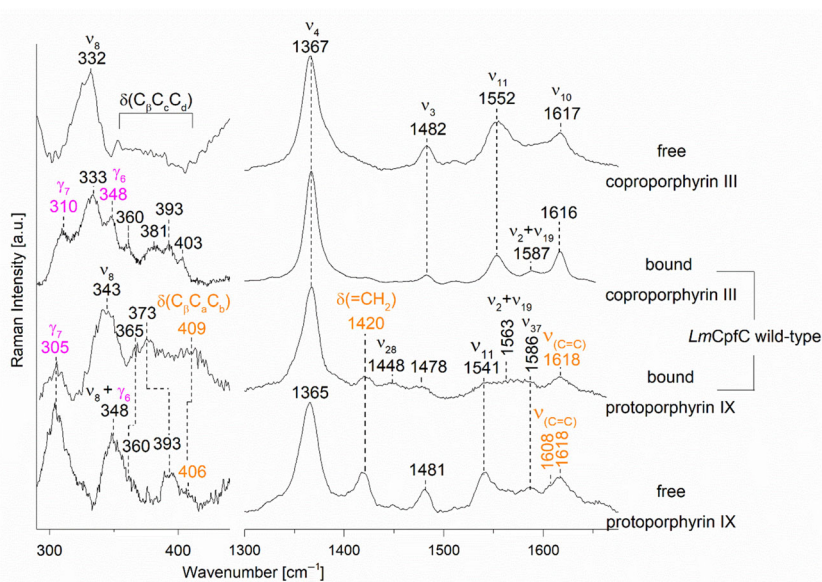


Fig. 5. Resonance Raman (RR) spectra in the low and high wavenumber regions of free cpIII (top), cpIII-bound WT *LmCpfC* [7], ppIX-bound WT *LmCpfC* and free ppIX (bottom). The RR out-of-plane band and the vinyl bending and stretching modes wavenumbers are reported in magenta and orange, respectively. The low wavenumber region of cpIII-bound WT *LmCpfC* was obtained with the 3600 grooves- mm^{-1} .

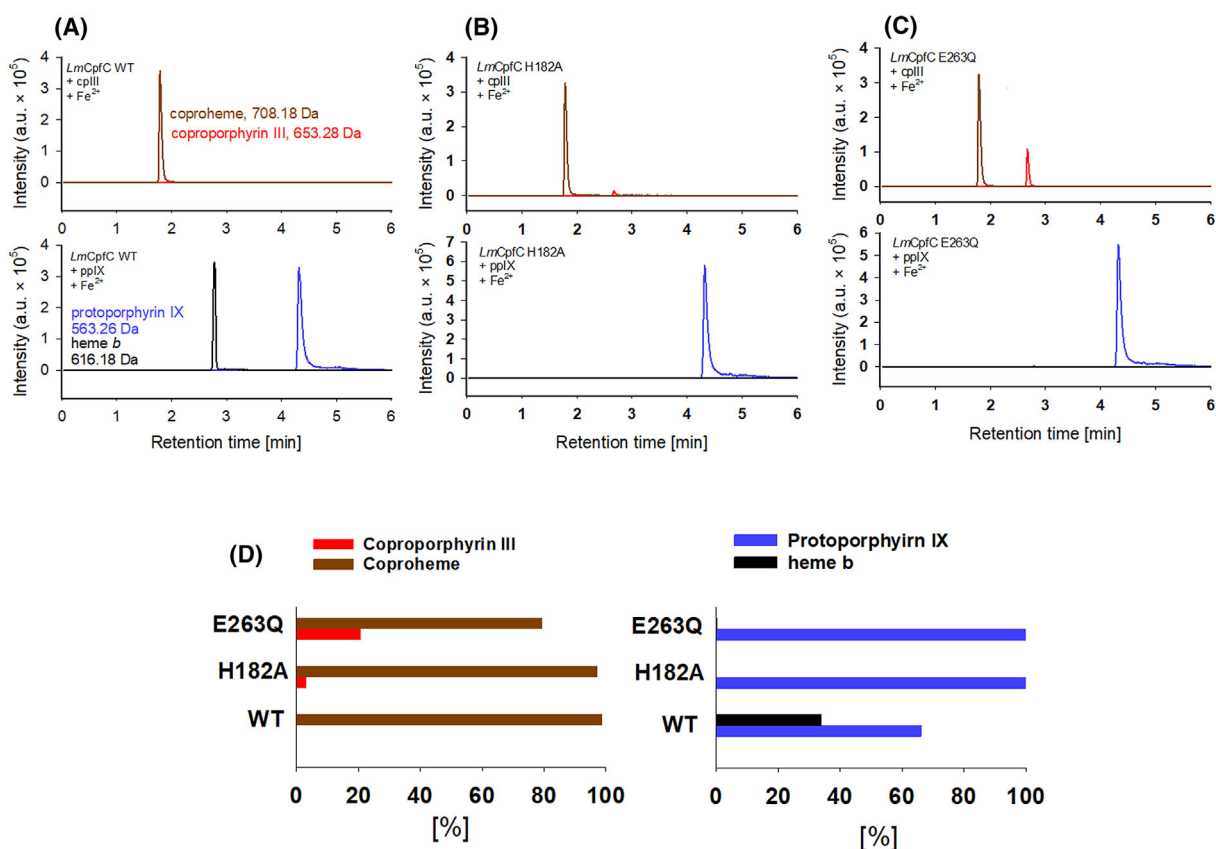


Fig. 6. LC-MS analysis of samples presented in Fig. 2. Chromatograms of samples eluting with a mass corresponding to coproheme (708.18 Da) are depicted in maroon, to cpIII (635.28 Da) in red, to heme *b* (616.18 Da) in black, and to pplx (563.26 Da) in blue. Chromatograms are presented for cpIII and pplx conversion by (A) WT, (B) H182A, and (C) E263Q variants of *LmCpfC*. (D) Quantification of coproheme (maroon), cpIII (red), heme *b* (black), and pplx (blue) in all respective samples, calculated by integration of the area under the respective elution peak.

H182A variant, as already observed by UV-vis spectroscopy, incompletely converts cpIII into coproheme and is unable to insert ferrous iron into pplx. E263Q variant had a lower efficiency of cpIII conversion, as more than 20% unreacted cpIII was detected in the corresponding sample.

Ferrous coproheme during turnover in *LmCpfC* variants

In Fig. 7, the final UV-vis spectra of the ferrous iron titrations, reported in Fig. 2A–C, are presented for the WT, H182A, and E263Q variants of *LmCpfC*, together with the spectra of the corresponding coproheme-bound species in their ferric and ferrous forms. Different from both the H182A and WT *LmCpfC*, the Soret band of the E263Q variant clearly shows, next to the peak maximum (407 nm), a shoulder at higher wavelengths (417 nm), characteristic of

ferrous coproheme (Figs 3 and 7) which is formed upon ferrous iron titration, and it is not readily oxidized to the final ferric coproheme product.

In order to verify the presence of ferrous coproheme in the cpIII-bound E263Q variant titrated with ferrous iron, we followed the metal titration also by RR spectroscopy (Fig. 8). The oxidation state of coproheme is monitored by the wavenumber of the ν_4 band. The chemically reduced coproheme (as obtained by the addition of sodium dithionite, Fig. 8, blue spectrum) exhibits a ν_4 band at 1358 cm^{-1} , which shifted to 1372 cm^{-1} in the ferric coproheme (green spectrum). During titration of E263Q *LmCpfC*, similar to the WT titration [29], a γ_{15} out-of-plane mode at 701 cm^{-1} is observed, not present either in the substrate or in the final ferric coproheme product. This latter band is characteristic of the formation of a stable ferric intermediate saddle distorted catalytic species [29]. In addition, the bands typical of the product in both the ferrous (ν_4 , ν_3 , and ν_{10} at 1358,

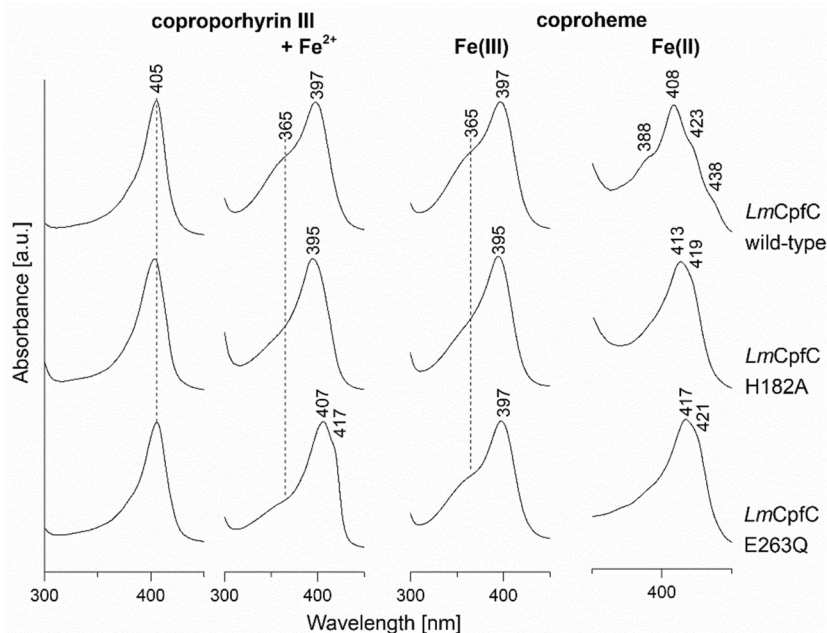


Fig. 7. Comparison of the final UV-vis spectra of the ferrous iron titrations with the corresponding spectra of the cpIII- and coproheme-bound species in their ferric and ferrous forms of wild-type (WT) and variants of *LmCpfC*.

1471, and 1609 cm^{-1} , respectively) and ferric (ν_4 , ν_3 , ν_2 , and ν_{10} at 1372, 1490, 1583 and 1627 cm^{-1} , respectively) species, together with those ascribed to the substrate (ν_4 , ν_{11} , and ν_{10} at 1367, 1552, and 1616 cm^{-1} , respectively) are clearly observed in the course of the titration. The ν_2 band of the ferrous product (at 1583 cm^{-1}) overlaps with the band at 1587 cm^{-1} ($\nu_2 + \nu_{19}$) of the cpIII-bound complex. On the other hand, these signatures were not present when titrating WT *LmCpfC* under identical conditions [29]. These results, therefore, imply that upon mutation of the distal glutamate (E283), ferrous coproheme cannot be fully oxidized to ferric coproheme as in the WT enzyme (Fig. 7).

Reduction potentials of wild-type *LmCpfC* and its variants

We found that the residues on the distal side are not essential for iron insertion (Figs 2 and 6) but influence the iron redox state of the coproheme product (Figs 7 and 8). This prompted us to determine the reduction potentials of the coproheme Fe(III)/Fe(II) redox couple in WT *LmCpfC* and its variants (Fig. 9). The WT protein exhibits the lowest redox potential of -206 mV of all the investigated samples. Mutation of the distal His-Glu pair exerts different effects on the reduction potential of the coproheme Fe(III)/Fe(II) redox couple, as the E^{ol} of H182A variant is only marginally higher than that of the WT protein

(-199 mV), whereas that of the E263Q variant is 27 mV more positive (-179 mV).

Discussion

The active site of protoporphyrin and coproporphyrin ferrochelatases is characterized by two conserved residues (His and Glu, throughout all taxa and phyla) on the distal side, whereas the residue on the proximal side is specific to phylogenetic clades (e.g., Met in eukaryotes, Tyr in Firmicutes, and Phe in Actinobacteria) [2,8]. The role of the glutamate-histidine pair has long been under investigation in ferrochelatases from prokaryotic, monoderm bacteria, and especially the histidine residue was believed to be essential for catalysis and involved in the initial iron binding [12,15]. The fundamental role of the distal histidine residue was observed when *BsCpfC* was studied using porphyrin substrates with two propionate groups, such as MppIX, N-MeMP, or ppIX [30]. The histidine residue was proposed to act as a distal base in the initial step in the iron insertion process, capable of deprotonating the porphyrin's pyrrole nitrogen atoms [22,31–34]. Here, we present data showing the inability of both the distal H182A and E263Q variants of *LmCpfC* to insert ferrous iron into protoporphyrin IX. However, all variants show activity when the physiological substrate (cpIII), is used in the assays (Figs 2 and 6). This observation questions the distal histidine's role in deprotonating the

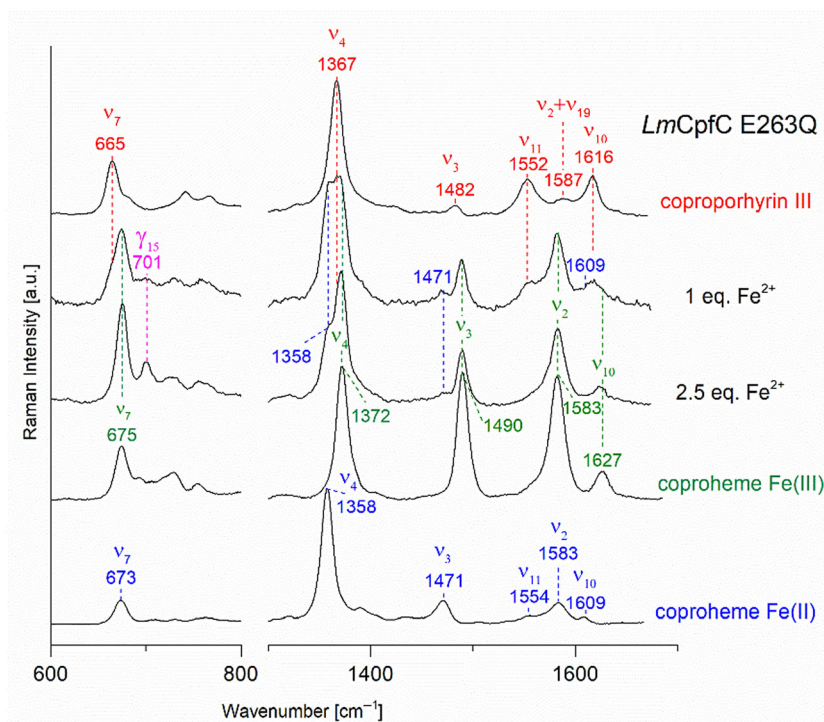


Fig. 8. Catalytic insertion of ferrous iron into cpIII by E263Q variant of *LmCpfC* followed by Resonance Raman spectroscopy (RR). RR spectra in the middle and high regions of cpIII-bound to E263Q variant, intermediate points during the titration and reconstituted coproheme-bound E263Q *LmCpfC*. The chemically reduced coproheme is also presented. The RR out-of-plane band wavenumbers are indicated in magenta, while in green, blue, and red are indicated the band wavenumbers typical of the coproheme ferric and ferrous form and cpIII complexes, respectively.

pyrrole nitrogen atoms, as this would be insensitive to the number of propionate groups of the porphyrin.

The reason for the reduced activity of the ppIX-bound WT and the complete loss of activity of its key distal variants is very likely to derive from an incorrect substrate binding, as a consequence of the presence of only two propionate substituents in the substrates. In fact, comparison of the structures, functional and spectroscopic studies of WT and mutated CpfCs from *Bacillus subtilis* in complex with *N*-MeMP or deuteroporphyrin IX 2,4-disulfonic acid dihydrochloride [15,35] with those of *LmCpfC* with coproheme and coproporphyrin III [5–7], clearly shows that the interaction of propionates at positions 2 and 4 with residues well buried in the protein core is fundamental for correct binding. The complete ferrous iron insertion also observed in this work by cpI-bound WT strengthens this conclusion. Porphyrins containing only two propionate groups are placed closer to the protein's surface, as the propionates at positions 6 and 7 are pointing to the solvent in all studied enzymes [5,15,24,35,36]. In addition, the comparison of the RR spectra of cpIII- and ppIX-bound

WT in this work points out the different propionate H-bond interactions, confirming that propionate groups at positions 6 and 7 have a weaker interaction in the ppIX ($360/393\text{ cm}^{-1}$) than in the cpIII complex ($381/393\text{ cm}^{-1}$) [7] (Fig. 5). This weaker binding in the two-propionate porphyrins may be responsible for the incomplete ferrous iron insertion into WT-protoporphyrin IX complex observed in this work. Furthermore, in the site-directed mutants, no catalytic activity remains when ppIX is used as a substrate (Figs 2 and 6).

The distal histidine residue (H182 in *LmCpfC*) was long believed to be responsible for deprotonating the nitrogen atoms of the pyrrole groups, a fundamental step in order to incorporate ferrous iron into the porphyrin macrocycle [22,31–34]. This deprotonation can be performed via a different mechanism in the distal variants when the physiological substrate cpIII is used, and the same holds true for cpI (Fig. 4). Binding of cpI in the correct spot strongly suggests that there are two propionate binding pockets with high affinity buried in the protein specific to CpfCs, which can be occupied by cpI and cpIII, anchoring propionates at

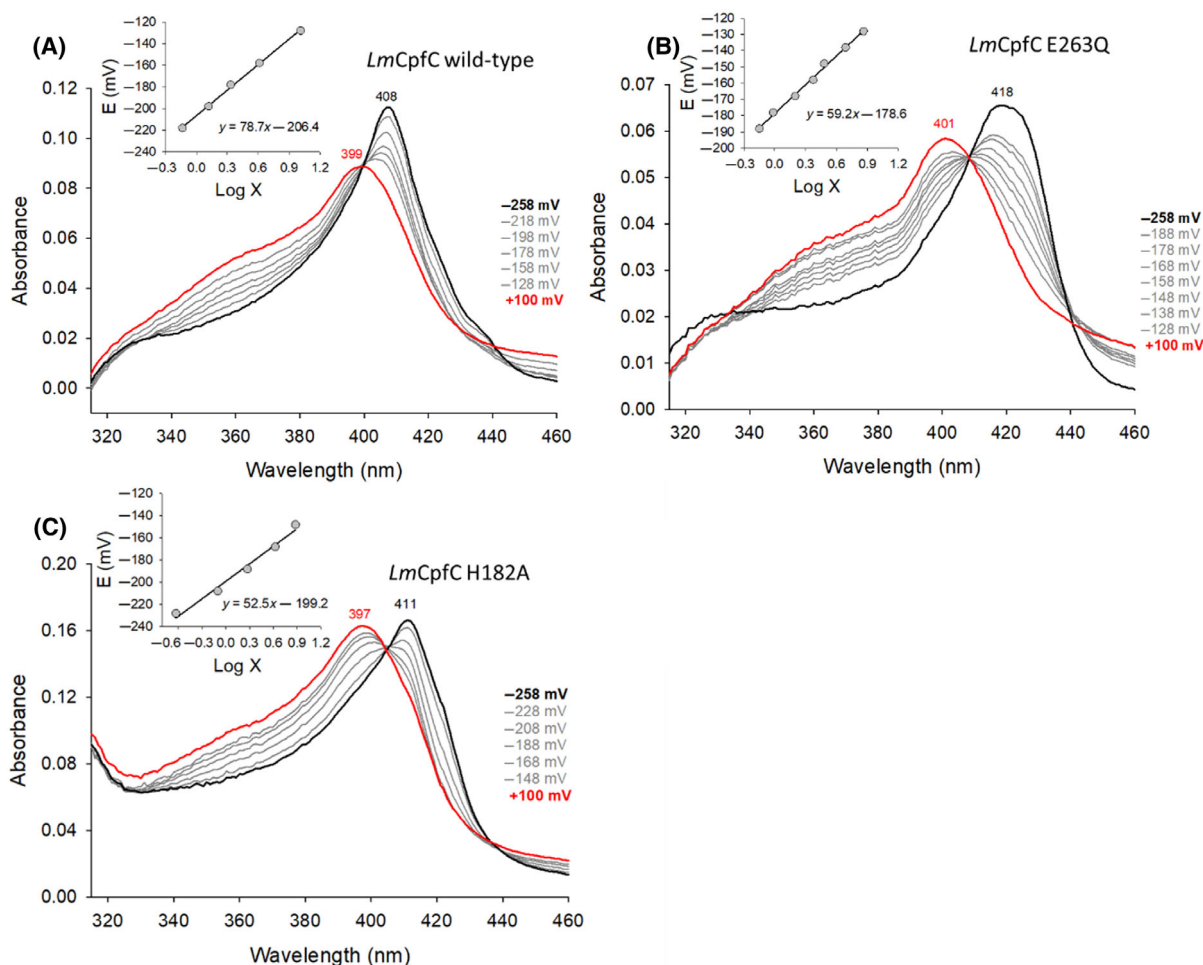


Fig. 9. Spectroelectrochemical determination of the reduction potentials of the Fe(III)/Fe(II) couple in (A) WT *LmCpfC* and (B) E263Q and (C) H182A variants of *LmCpfC*. The spectra of protein-bound ferric and ferrous coproHEME are shown as red and black lines, respectively. Intermediate spectra are represented in gray. The respective applied potentials are listed in the plots. Insets depict the Nernst plot of each redox titration versus SHE. We noted that the spectral characteristics obtained by electrochemical titration are not identical to those obtained in HEPES buffer at pH 7.4, as reported in Fig. 7, due to the different buffer conditions (see [Materials and methods](#)). Titrations have been measured in triplicates ($n = 3$), with one representative titration presented for each sample.

positions 2 and 4 (Fig. 1) [7]. These two propionates are not present in ppIX, which suggests an involvement of these functional groups in the essential step of pyrrole nitrogen deprotonation that has to be investigated in future studies.

Although neither H182 nor E283 are essential for catalysis using cpIII, the active site architecture plays a significant role in the process of iron oxidation. Only ferrous iron can be inserted by ferrochelatases into porphyrins, but the product is always ferric coproHEME, even when the reaction is performed under completely anaerobic conditions [6,29]. The subsequent and last enzyme involved in the CPD pathway, coproHEME decarboxylase, depends on ferric coproHEME as a redox-active substrate in order to facilitate the final

cleavage of propionates at positions 2 and 4 to vinyl groups to give heme *b*, the ultimate product of this pathway [26].

The exact mechanism of oxidation and the identity of acceptor of the electron from the ferrous iron are not clear to date. Nevertheless, we have identified E263 as a residue of interest, as it is definitely involved in this process, and contributes significantly to the reduction potential of the Fe(III)/Fe(II) redox couple of the protein-bound coproHEME. Indeed, the E263Q variant exhibits the highest potential, and therefore, its ferric form is less stabilized compared to the WT species, in agreement with the observed incomplete oxidation of ferrous coproHEME to ferric coproHEME. The exact reason why the E263Q variant is unable to fully

convert cpIII into coproheme is not clear, but it can be speculated that the lack of the negatively charged amino acid side chain in the active site decreases the capability to attract the positively charged ferrous iron. Future studies will be needed to further dissect and investigate the molecular features of the active site of *LmCpfC*, which facilitates proton abstraction from the pyrrole nitrogen atoms and the oxidation to yield ferric coproheme as the final product.

Materials and methods

Generation, expression, and purification of WT and variants of *LmCpfC*

The variants H182A and E263Q were generated by site-directed mutagenesis according to the manufacturer's protocol using the available plasmid pET21a(+) with the *LmCpfC* wild-type sequence and a 6 × His-tag (5) as a template (see Table 1 for Primers). The reaction mixture was DpnI digested and then 2 μL was used to heat-shock transform *Escherichia coli* XL-10 according to the Agilent Technologies protocol. Single colonies were picked and overnight cultures were inoculated from which the plasmids were harvested on the next day using the Monarch Plasmid Miniprep Kit (New England Biolabs, Frankfurt/Main, Germany). The plasmids were analyzed by SANGER Sequencing done by Microsynth AG (Vienna, Austria) to confirm the introduced mutations. Correct plasmids were re-transformed into the expression strain *E. coli* BL21 GOLD. Expression cultures did grow in LB medium supplemented with 1 mM ampicillin and at 37 °C until an OD₆₀₀ of approx. 0.6 was reached. Then, the cultures were cooled to 24 °C, then induced by adding 0.5 mM IPTG and further cooled down to 20 °C for overnight expression. On the next morning, the cells were harvest by centrifugation (2430 g). The cell pellets were lysed by sonication (SONOPLUS Bandelin, Berlin, Germany) in a lysis buffer and cell debris were removed by another centrifugation step (38 724 g). The lysate was filtered and applied to a 5-mL HisTrap FF column (Cytiva, Sweden, Uppsala). Gradient for elution was 0–500 mM Imidazole over 60 min. The

Table 1. Primers designed for site-directed mutagenesis to create *LmCpfC* variants.

Primer name	Primer sequence
<i>LmCpfC</i>	5-atactgttttaattgtttccgcagccagttgcccagagaaaatta
H182A_fw	aacaaca-3
<i>LmCpfC</i>	5-tgtgtttaaattttctctctggcaactggctgcggaacaattaa
H182A_rev	aacagtat-3
<i>LmCpfC</i>	5-ggatttggcagaacatttcaagggttttatatgataatgattat
E263Q_fw	gaatgtaaag-3
<i>LmCpfC</i>	5-ctttacattcataatcattatcatataaacctgtaaatgttctgc
E263Q_rev	cacaaatcc-3

Sequence alterations are shown in red.

pooled fractions containing *LmCpfC* were buffer exchanged to a 1 × PBS buffer pH 7.4 with 100 mM NaCl using a PD-10 column (Cytiva, Amersham, UK) and stored at –80 °C.

Sample preparation and ferrous iron insertion

Protoporphyrin IX (ppIX), coproporphyrin I (cpI), and coproporphyrin III (cpIII) were purchased from Frontiers Scientific (Logan, UT, USA; product numbers: P563-9 and C654-3). The lyophilized powder was dissolved in 0.5 M NaOH and the stock concentration was determined by using an extinction coefficient for free ppIX of 86.168 M⁻¹·cm⁻¹ and for free cpIII of 150.736 M⁻¹·cm⁻¹ [6]. PpIX, cpI, or cpIII was added in 50-mM HEPES buffer pH 7.4 and then titrated with the apo-*LmCpfC* until no spectral changes were visible. The same results are observed, if the ppIX was dissolved in 0.5 M NaOH and DMSO (1 : 1 ratio) and then diluted in HEPES buffer (95% of HEPES buffer), before the titration with the apoprotein.

For the iron insertion, a 1-mM ferrous iron [source: iron (II) sulfate heptahydrate; CAS: 7782-62-0; LOT # SLCH2225; Sigma, Vienna, Austria] stock was prepared freshly with argon-flushed ddH₂O, in a Whitley DG250 Anaerobic Workstation (Don Whitley Scientific, Bingley, UK) under anaerobic conditions for all titrations individually and 5 μL transferred to PCR tube. Each PCR tube was used for only one iron titration point to avoid unwanted oxidation in between steps. We added 2.5 μM steps of ferrous iron to 5 μM of ppIX, cpI, or cpIII, in the PCR tubes to the protein complex solution, previously degassed with nitrogen gas. To complete the reaction, we waited for 3 min for each step. The titration was stopped at a 1.5-fold excess of ferrous iron over added *LmCpfC* and 20 μL of each mixture was transferred to a fresh 1.5 mL reaction tube for mass spectrometric analysis of the porphyrin species and content. For details on the RR measurements, see Ref. [29]. No spectral changes have been observed within an hour of preparation. For the E263Q *LmCpfC*, the addition of ferrous iron to the sample above 2.5 eq. of Fe²⁺ does not further change the spectrum.

The ferrous form of the E263Q *LmCpfC* coproheme-bound species was prepared by flushing the ferric coproheme complex with nitrogen gas and, then, by reducing it with a freshly prepared sodium dithionite solution (20 mg·mL⁻¹). For the RR experiments, the concentration was in the range of 18–40 μM for all the samples and was determined as reported in References [6,7]. Only for the free and bound ppIX was used a concentration in the range of 5–10 μM.

UV–vis electronic absorption spectroscopy

UV–vis electronic absorption was obtained at room temperature using a 1-cm cuvette or a 5-mm NMR tube using a Cary 60 spectrophotometer (Agilent Technologies, Santa Clara, CA, USA) with a resolution of 1.5 nm and a scan

Table 2. Summary of the excitation wavelength, the power on the sample, the total integration time (in minutes), and number of averaged RR spectra reported in this work. The spectra were obtained at low resolution (grating: 1800 grooves-mm⁻¹), if otherwise indicated instead were obtained at high resolution (grating: 3600 grooves-mm⁻¹).

Sample	Laser power on the sample (mW)	Excitation wavelength (nm)	Low resolution (average per integration time)
Coproporphyrin III E263Q	1.0	413.1	8 spectra per 40 min
Ferric coproheme E263Q	7.0	404.8	2 spectra per 10 min
Ferrous coproheme E263Q	2.5	413.1	3 spectra per 15 min
Coproporphyrin III E263Q + 1.0 eq. of Fe ²⁺	1.0	413.1	10 spectra per 10 min
Coproporphyrin III E263Q + 2.5 eq. of Fe ²⁺	1.0	413.1	30 spectra per 30 min
Free coproporphyrin III	2.0	404.8	64 spectra per 320 min
Free protoporphyrin IX	2.0	404.8	7 spectra per 35 min
Coproporphyrin III WT	1.0	413.1	110 spectra per 110 min (50 spectra per 250 min in high resolution)
Protoporphyrin IX WT	2.0	413.1	20 spectra per 20 min

rate of 300 nm·min⁻¹. All the spectra were normalized to the maximum intensity of the Soret band and the 450–700 nm region has been magnified to allow better visualization, as indicated in the figures.

Porphyrin species and content analysis by mass spectrometry

4 µL of the protein complex solution was directly injected into a LC-ESI-MS system (LC: Agilent 1290 Infinity II UPLC). A gradient from 15 to 80% acetonitrile in 0.1% formic acid (using a Waters BioResolve column (2.1 × 5 mm)) at a flow rate of 400 µL·min⁻¹ was applied (9-min gradient time). Detection was performed with a TOF instrument (Agilent Series 6230 LC-TOFMS) equipped with the Jetstream ESI source in positive ion, MS mode (range: 100–3000 m/z). Instrument calibration was performed using ESI calibration mixture (Agilent). Two blank runs (injection of 5-µL MS-grade water) were performed prior to the injection of the samples and one was performed in between each sample in order to avoid carry-over from previous measurements. Data were processed using MASSHUNTER BIOCONFIRM B.08.00 (Agilent) and the spectrum was deconvoluted by MAXENT. For the heme derivatives, the relative proportions were calculated by comparing the areas of the EICs of the monoisotopic masses. SKYLINE (64-bit) (MacCoss Lab Software, Seattle, WA, USA) 21.2.0.425 was used.

Resonance Raman (RR) spectroscopy

The RR spectra were obtained by placing the samples in a slowly rotating 5 mm NMR tube and using the 404.8 nm laser line of a MatchBox Series diode laser (Integrated Optics, Vilnius, Lithuania) or the 413.1 nm laser line of an Innova300C Kr⁺ laser (Coherent, Santa Clara, CA, USA). The setup has been previously described in Gabler

et al. [29]. For all the experiments, a grating of 1800 grooves-mm⁻¹ was used with a nominal resolution of 4 cm⁻¹, unless otherwise stated.

The UV–vis spectra were recorded both before and after RR measurements to ensure that no degradation of the sample occurred under the experimental conditions. The RR spectra were calibrated using indene and carbon tetrachloride as standards to an accuracy of 1 cm⁻¹ for intense isolated bands. To ensure reproducibility and to improve the signal-to-noise ratio, all the measurements were repeated several times and summed if no spectral differences were noted. The laser power on the sample, the integration time, and the number of averaged spectra reported in the figures are summarized in Table 2. All the spectra were baseline-corrected, normalized to the intensity of the ν₈ (332–346 cm⁻¹) or the ν₄ band (1358–1372 cm⁻¹) depending on the wavenumber region. For the spectra obtained in DMSO (Fig. 5), the DMSO was subtracted.

Determination of the reduction potential by spectroelectrochemistry

Spectroelectrochemical titrations were performed using a homemade OTTLE (optically transparent thin layer spectroelectrochemical) cell [37]. The three-electrode configuration consisted of a gold mini-grid working electrode (Buckbee-Mears), a silver chloride microreference electrode (AMEL Electrochemistry), separated from the working solution by a Vycor set, and a platinum wire as counter-electrode. All potentials are referenced to the standard hydrogen electrode SHE. Potentials were applied across the OTTLE cell with an Amel model 2053 potentiostat/galvanostat. UV–vis spectra were recorded using a Varian Cary C50 spectrophotometer. All experiments were performed at 25 °C in an oxygen-free environment, obtained by flushing the OTTLE cell with argon. Constant temperature was maintained by a circulating water bath.

Experiments were performed using 6- to 17- μM protein complex solutions in 100-mM phosphate buffer plus 50 mM NaCl, pH 7.0; 40 μM methyl viologen and a mixture of 2 μM lumiflavine-3-acetate, methylene blue, phenazine methosulfate, and indigo disulfonate were used as redox mediators.

Acknowledgements

This project was financed by the Austrian Science Fund, FWF, projects P33544, P36967, W1224 (SH) and Fondazione Cassa di Risparmio di Firenze, grant 2020.1397 (GS). This project was supported by the EQ-BOKU VIBT GmbH and the BOKU Core Facility Mass Spectrometry, and MUR-Italy (“Progetto Dipartimenti di Eccellenza 2023–2027”, CUP B97G22000740001 – DICUS 2.0) allocated to the Department of Chemistry “Ugo Schiff” (FS, MB, GS). AD is the recipient of a Ph.D. fellowship funded by MUR-Italy “Progetto Dipartimenti di Eccellenza 2018–2022”, CUP B96C1700020008, allocated to the Department of Chemistry “Ugo Schiff”.

Conflict of interest

The authors declare no conflict of interest.

Author contributions

SH and GS planned experiments; TG, AD, MBel, and FS performed experiments; TG, AD, MBel, FS, MBec, GB, PGF, GS, and SH analyzed data; TG, AD, MBel, FS, MBec, GB, PGF, GS, and SH wrote the paper.

Peer review

The peer review history for this article is available at <https://www.webofscience.com/api/gateway/wos/peer-review/10.1111/febs.17101>.

Data availability statement

All relevant data have been deposited to a repository (<https://zenodo.org/records/10682116>).

References

- 1 Dailey HA, Gerdes S, Dailey TA, Burch JS & Phillips JD (2015) Noncanonical coproporphyrin-dependent bacterial heme biosynthesis pathway that does not use protoporphyrin. *Proc Natl Acad Sci USA* **112**, 2210–2215.
- 2 Dailey HA, Dailey TA, Gerdes S, Jahn D, Jahn M, O'Brian MR & Warren MJ (2017) Prokaryotic Heme

biosynthesis: multiple pathways to a common essential product. *Microbiol Mol Biol Rev* **81**, e00048-16.

- 3 Layer G (2021) Heme biosynthesis in prokaryotes. *Biochim Biophys Acta Mol Cell Res* **1868**, 118861.
- 4 Dailey HA, Dailey TA, Wu CK, Medlock AE, Wang KF, Rose JP & Wang BC (2000) Ferrochelatase at the millennium: structures, mechanisms and [2Fe-2S] clusters. *Cell Mol Life Sci* **57**, 1909–1926.
- 5 Hofbauer S, Helm J, Obinger C, Djinić-Carugo K & Furtmüller PG (2020) Crystal structures and calorimetry reveal catalytically relevant binding mode of coproporphyrin and coproheme in coproporphyrin ferrochelatase. *FEBS J* **287**, 2779–2796.
- 6 Gabler T, Sebastiani F, Helm J, Dali A, Obinger C, Furtmüller PG, Smulevich G & Hofbauer S (2022) Substrate specificity and complex stability of coproporphyrin ferrochelatase is governed by hydrogen-bonding interactions of the four propionate groups. *FEBS J* **289**, 1680–1699.
- 7 Dali A, Gabler T, Sebastiani F, Destinger A, Furtmüller PG, Pfanzagl V, Becucci M, Smulevich G & Hofbauer S (2023) Active site architecture of coproporphyrin ferrochelatase with its physiological substrate coproporphyrin III: propionate interactions and porphyrin core deformation. *Protein Sci* **32**, e4534.
- 8 Weerth RS, Medlock AE & Dailey HA (2021) Ironing out the distribution of [2Fe-2S] motifs in ferrochelatases. *J Biol Chem* **297**, 101017.
- 9 Shepherd M, Dailey TA & Dailey HA (2006) A new class of [2Fe-2S]-cluster-containing protoporphyrin (IX) ferrochelatases. *Biochem J* **397**, 47–52.
- 10 Pfanzagl V, Holcik L, Maresch D, Gorgone G, Michlits H, Furtmüller PG & Hofbauer S (2018) Coproheme decarboxylases – phylogenetic prediction versus biochemical experiments. *Arch Biochem Biophys* **640**, 27–36.
- 11 Dailey HA & Medlock AE (2022) A primer on heme biosynthesis. *Biol Chem* **403**, 985–1003.
- 12 Hansson MD, Karlberg T, Rahardja MA, Al-Karadaghi S & Hansson M (2007) Amino acid residues His183 and Glu264 in *Bacillus subtilis* ferrochelatase direct and facilitate the insertion of metal ion into protoporphyrin IX. *Biochemistry* **46**, 87–94.
- 13 Wang Y & Shen Y (2013) Is it possible for Fe²⁺ to approach protoporphyrin IX from the side of Tyr-13 in *Bacillus subtilis* ferrochelatase? An answer from QM/MM study. *J Mol Model* **19**, 963–971.
- 14 Hansson MD, Karlberg T, Söderberg CA, Rajan S, Warren MJ, Al-Karadaghi S, Rigby SE & Hansson M (2011) Bacterial ferrochelatase turns human: Tyr13 determines the apparent metal specificity of *Bacillus subtilis* ferrochelatase. *J Biol Inorg Chem* **16**, 235–242.
- 15 Karlberg T, Hansson MD, Yengo RK, Johansson R, Thorvaldsen HO, Ferreira GC, Hansson M & Al-Karadaghi S (2008) Porphyrin binding and distortion

- and substrate specificity in the ferrochelatase reaction: the role of active site residues. *J Mol Biol* **378**, 1074–1083.
- 16 Franco R, Ma JG, Lu Y, Ferreira GC & Shelnett JA (2000) Porphyrin interactions with wild-type and mutant mouse ferrochelatase. *Biochemistry* **39**, 2517–2529.
 - 17 Hoggins M, Dailey HA, Hunter CN & Reid JD (2007) Direct measurement of metal ion chelation in the active site of human ferrochelatase. *Biochemistry* **46**, 8121–8127.
 - 18 Medlock A, Swartz L, Dailey TA, Dailey HA & Lanzilotta WN (2007) Substrate interactions with human ferrochelatase. *Proc Natl Acad Sci USA* **104**, 1789–1793.
 - 19 Karlberg T, Lecerof D, Gora M, Silvegren G, Labbe-Bois R, Hansson M & Al-Karadaghi S (2002) Metal binding to *Saccharomyces cerevisiae* ferrochelatase. *Biochemistry* **41**, 13499–13506.
 - 20 Hunter GA, Sampson MP & Ferreira GC (2008) Metal ion substrate inhibition of ferrochelatase. *J Biol Chem* **283**, 23685–23691.
 - 21 Gora M, Grzybowska E, Rytka J & Labbe-Bois R (1996) Probing the active-site residues in *Saccharomyces cerevisiae* ferrochelatase by directed mutagenesis. In vivo and in vitro analyses. *J Biol Chem* **271**, 11810–11816.
 - 22 Sellers VM, Wu CK, Dailey TA & Dailey HA (2001) Human ferrochelatase: characterization of substrate-iron binding and proton-abstracting residues. *Biochemistry* **40**, 9821–9827.
 - 23 Medlock AE, Dailey TA, Ross TA, Dailey HA & Lanzilotta WN (2007) A pi-helix switch selective for porphyrin deprotonation and product release in human ferrochelatase. *J Mol Biol* **373**, 1006–1016.
 - 24 Medlock AE, Najahi-Missaoui W, Shiferaw MT, Albetel AN, Lanzilotta WN & Dailey HA (2021) Insight into the function of active site residues in the catalytic mechanism of human ferrochelatase. *Biochem J* **478**, 3239–3252.
 - 25 Celis AI, Gauss GH, Streit BR, Shisler K, Moraski GC, Rodgers KR, Lukat-Rodgers GS, Peters JW & DuBois JL (2017) Structure-based mechanism for oxidative decarboxylation reactions mediated by amino acids and Heme propionates in Coproheme decarboxylase (HemQ). *J Am Chem Soc* **139**, 1900–1911.
 - 26 Milazzo L, Gabler T, Pühringer D, Jandova Z, Maresch D, Michlits H, Pfanzagl V, Djinić-Carugo K, Oostenbrink C, Furtmüller PG *et al.* (2019) Redox cofactor rotates during its stepwise decarboxylation: molecular mechanism of conversion of Coproheme to Heme. *ACS Catal* **9**, 6766–6782.
 - 27 Michlits H, Lier B, Pfanzagl V, Djinić-Carugo K, Furtmüller PG, Oostenbrink C, Obinger C & Hofbauer S (2020) Actinobacterial coproheme decarboxylases use histidine as distal base to promote compound I formation. *ACS Catal* **10**, 5405–5413.
 - 28 Sebastiani F, Michlits H, Lier B, Becucci M, Furtmüller PG, Oostenbrink C, Obinger C, Hofbauer S & Smulevich G (2021) Reaction intermediate rotation during the decarboxylation of coproheme to heme b in *C. Diphtheriae*. *Biophys J* **120**, 3600–3614.
 - 29 Gabler T, Dali A, Sebastiani F, Furtmüller PG, Becucci M, Hofbauer S & Smulevich G (2023) Iron insertion into coproporphyrin III-ferrochelatase complex: evidence for an intermediate distorted catalytic species. *Protein Sci* **32**, e4788.
 - 30 Dailey HA & Gerdes S (2015) HemQ: An iron-coproporphyrin oxidative decarboxylase for protoheme synthesis in Firmicutes and Actinobacteria. *Arch Biochem Biophys* **574**, 27–35.
 - 31 Hunter GA & Ferreira GC (2022) Metal ion coordination sites in ferrochelatase. *Coord Chem Rev* **460**, 214464.
 - 32 Wu CK, Dailey HA, Rose JP, Burden A, Sellers VM & Wang BC (2001) The 2.0 Å structure of human ferrochelatase, the terminal enzyme of heme biosynthesis. *Nat Struct Biol* **8**, 156–160.
 - 33 Asuru AP, An M & Busenlehner LS (2012) Dissection of porphyrin-induced conformational dynamics in the heme biosynthesis enzyme ferrochelatase. *Biochemistry* **51**, 7116–7127.
 - 34 Wu J, Wen S, Zhou Y, Chao H & Shen Y (2016) Human Ferrochelatase: insights for the mechanism of ferrous iron approaching Protoporphyrin IX by QM/MM and QTCP free energy studies. *J Chem Inf Model* **56**, 2421–2433.
 - 35 Lecerof D, Fodje M, Hansson A, Hansson M & Al-Karadaghi S (2000) Structural and mechanistic basis of porphyrin metallation by ferrochelatase. *J Mol Biol* **297**, 221–232.
 - 36 Franco R, Al-Karadaghi S & Ferreira GC (2011) Resonance Raman spectroscopic examination of Ferrochelatase-induced porphyrin distortion. *J Porphyr Phthalocyanines* **15**, 357–363.
 - 37 Hofbauer S, Gysel K, Bellei M, Hagemüller A, Schaffner I, Mlynek G, Kostan J, Pirker KF, Daims H, Furtmüller PG *et al.* (2014) Manipulating conserved heme cavity residues of chlorite dismutase: effect on structure, redox chemistry, and reactivity. *Biochemistry* **53**, 77–89.